Supporting information

Studies of CO_2 Hydrogenation over Cobalt/Ceria Catalysts with *in situ* Characterization: The Effect of Cobalt Loading and Metal-Support Interactions on the Catalytic Activity

Kaixi Deng[1], Lili Lin[2], Ning Rui[2], Dimitriy Vovchok[2], Feng Zhang[3], Shuhao Zhang[3], Sanjaya Senanayake[2], Taejin Kim[3], Jose A. Rodriguez[1,2]

1. Department of Chemistry, Stony Brook University, Stony Brook, NY 11794, USA
2. Chemistry Division, Brookhaven National Laboratory, Upton, NY 11973, USA
3. Materials Science and Chemical Engineering Department, Stony Brook University, Stony Brook, NY 11794, USA

Table of Contents

XRD section

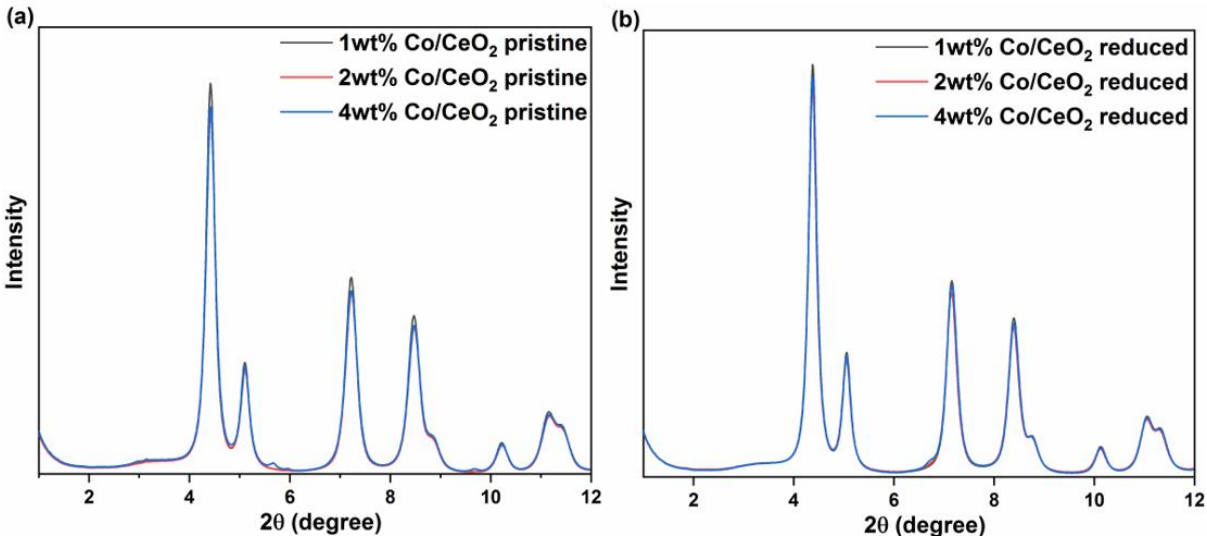

Figure S1.A. Full XRD patterns for (a) pristine and (b) reduced Co/CeO2 samples

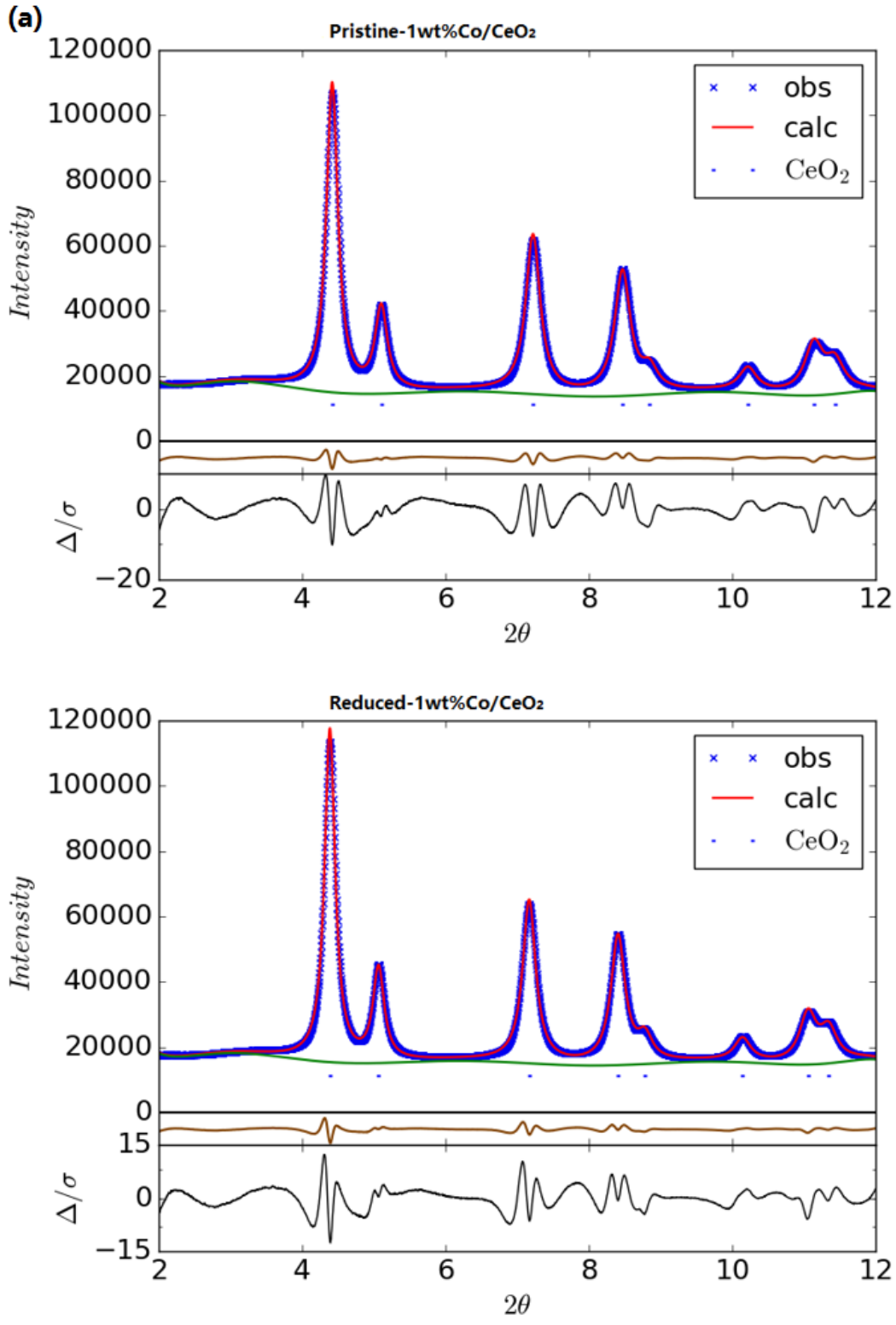
(a)
Pristine-1wt%Co/CeO2
obs
calc
CeO2
Intensity
Δ/σ
2θ
Reduced-1wt%Co/CeO2
obs
calc
CeO2
Intensity
Δ/σ
2θ

(b)

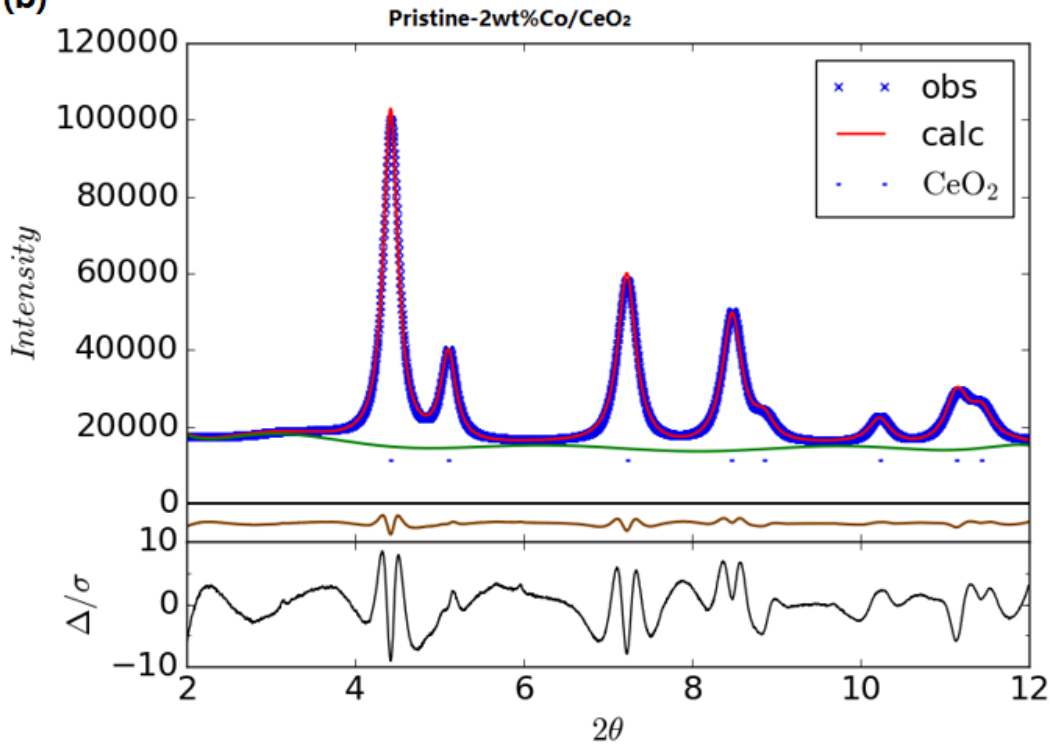
Pristine-2wt%Co/CeO₂
obs
calc
CeO2
Intensity
Δ/σ
2θ

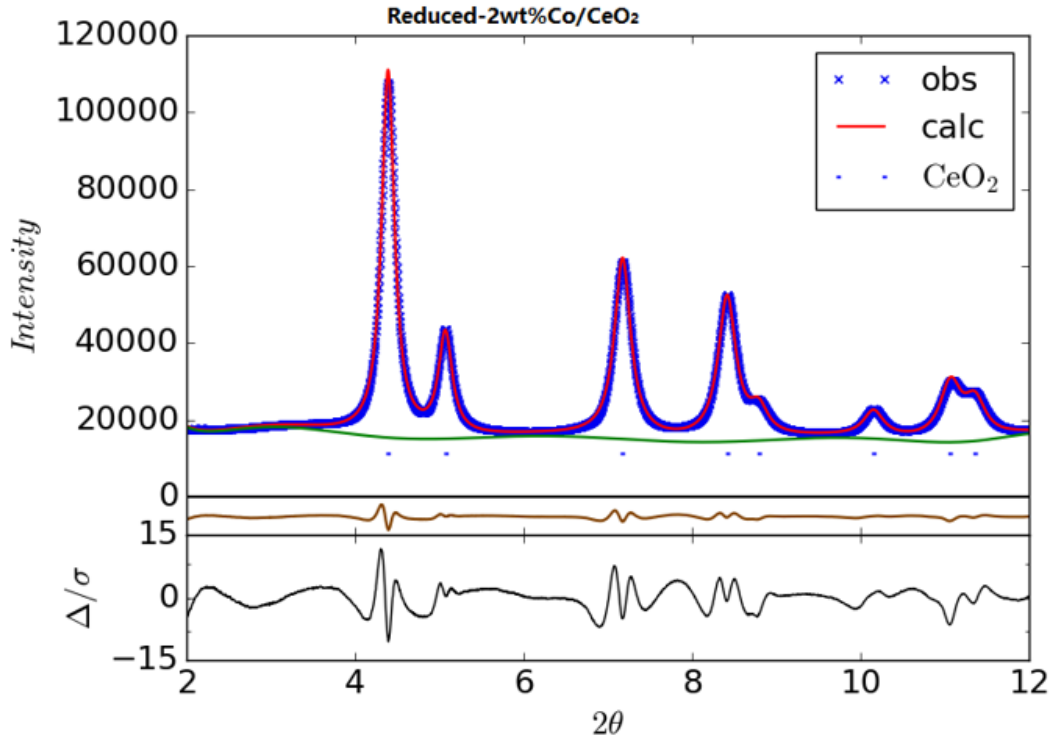
Reduced-2wt%Co/CeO₂
obs
calc
CeO2
Intensity
Δ/σ
2θ

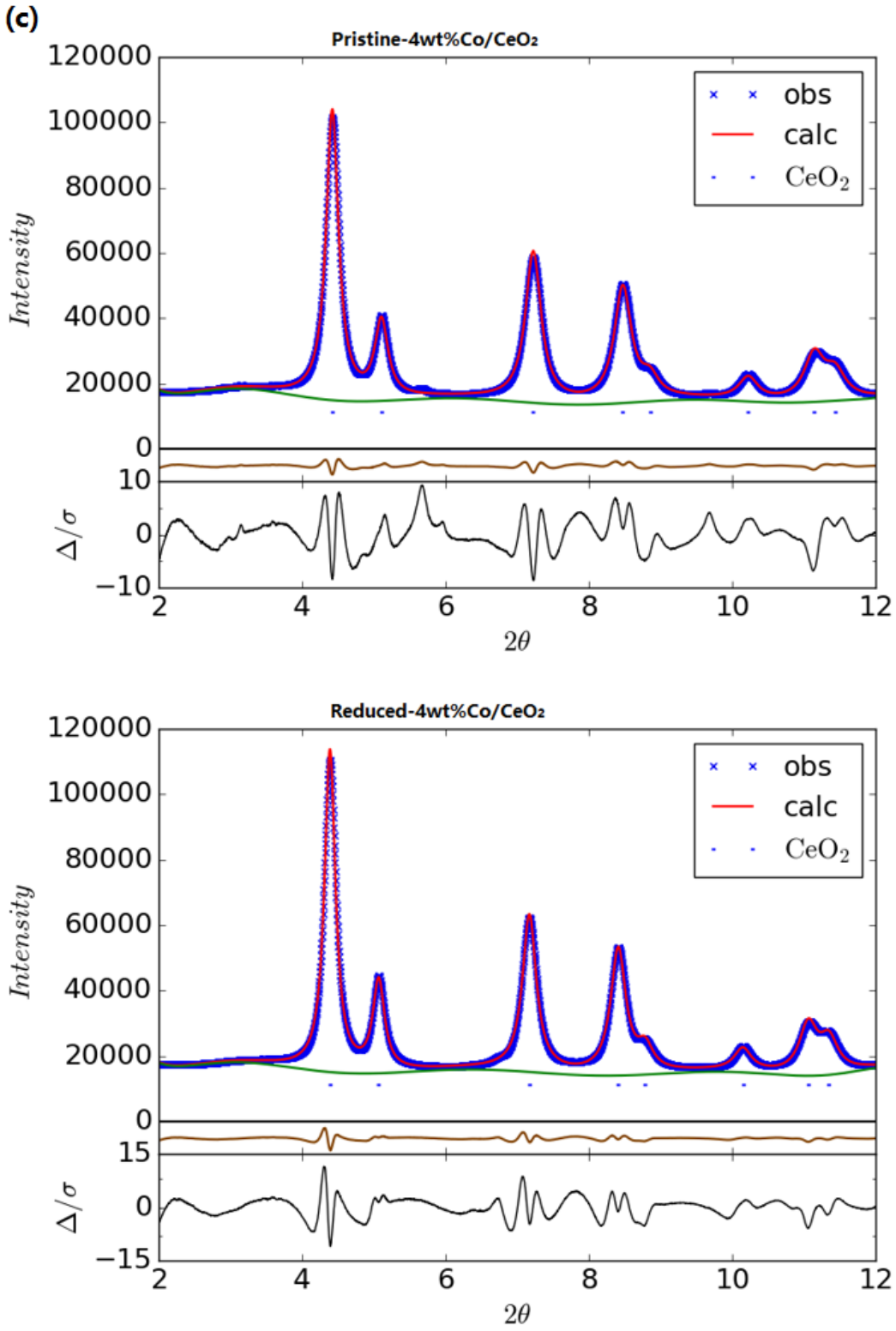

Figure S1.B. Rietveld refinement results for the CeO_2 phase in pristine or reduced conditions for (a) 1wt% Co/CeO_2 (b) 2wt% Co/CeO_2 (c) 4wt% Co/CeO_2 catalysts.

Table S1. Rietveld refinement results for the CeO_2 phase in pristine and reduced Co/CeO_2 catalysts.

Sample	CeO_2 Lattice constant (Å)	CeO_2 Crystal size (nm)	CeO_2 microstrain (%)	Data residual
Pristine-1wt% Co/CeO_2-25 ℃	5.4114	12	3.42	1.94 %
Reduced-1wt% Co/CeO_2-250 ℃	5.4513	14	3.34	1.92 %
Pristine-2wt% Co/CeO_2-25 ℃	5.4079	12	3.66	1.84%
Reduced-2wt% Co/CeO_2-250 ℃	5.4456	14	3.56	1.67 %
Pristine-4wt% Co/CeO_2-25 ℃	5.4086	12	3.52	1.84 %
Reduced-4wt% Co/CeO_2-250 ℃	5.4492	14	3.59	1.72 %

NAP-XPS Section

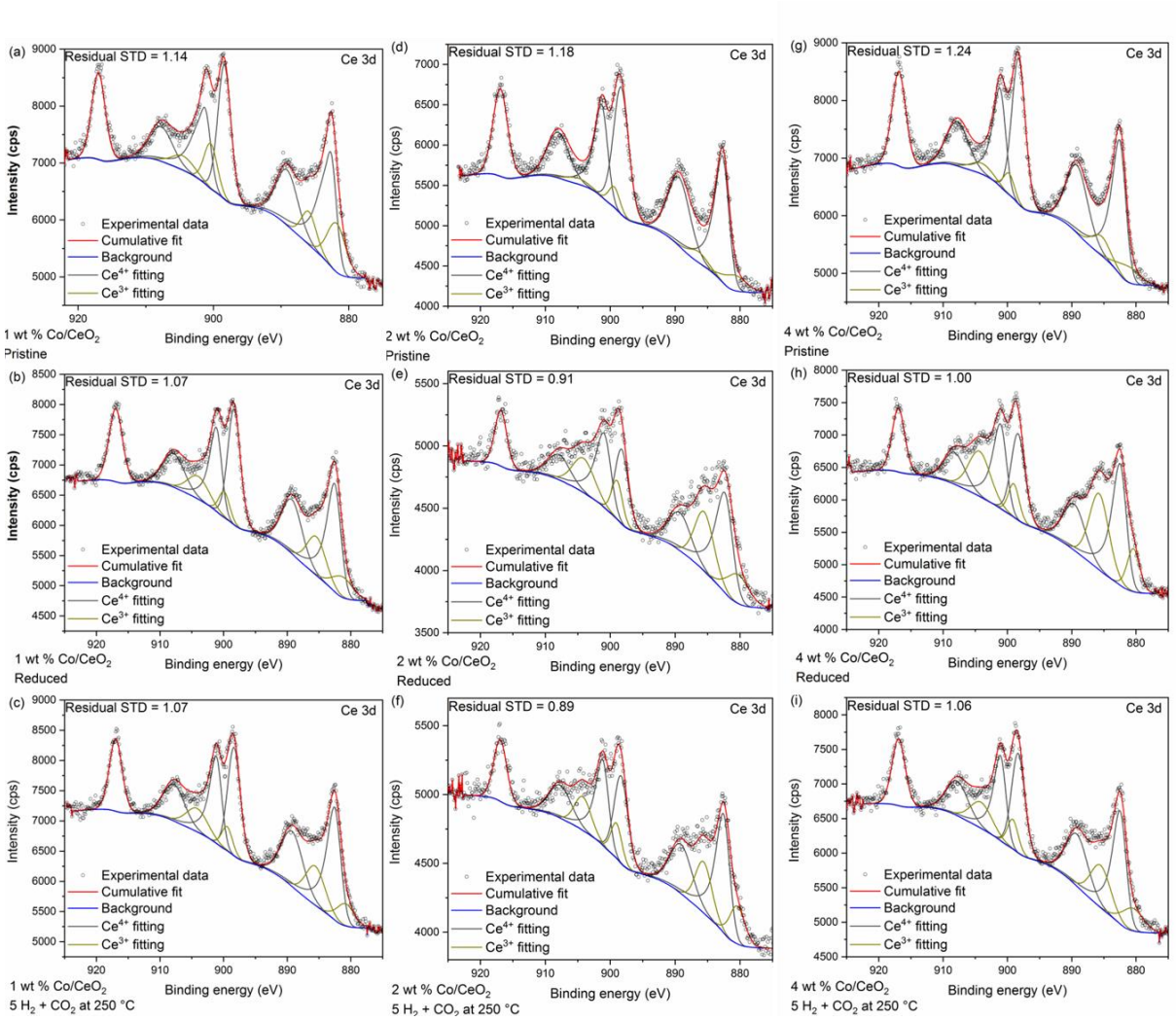

Figure S2. peak deconvolution fitting results for 1wt% Co/CeO2 (a, b, c), 2wt% Co/CeO2 (d, e, f), and 4wt% Co/CeO2 (g, h, i) at pristine, reduced and *in situ* conditions.

XANES section

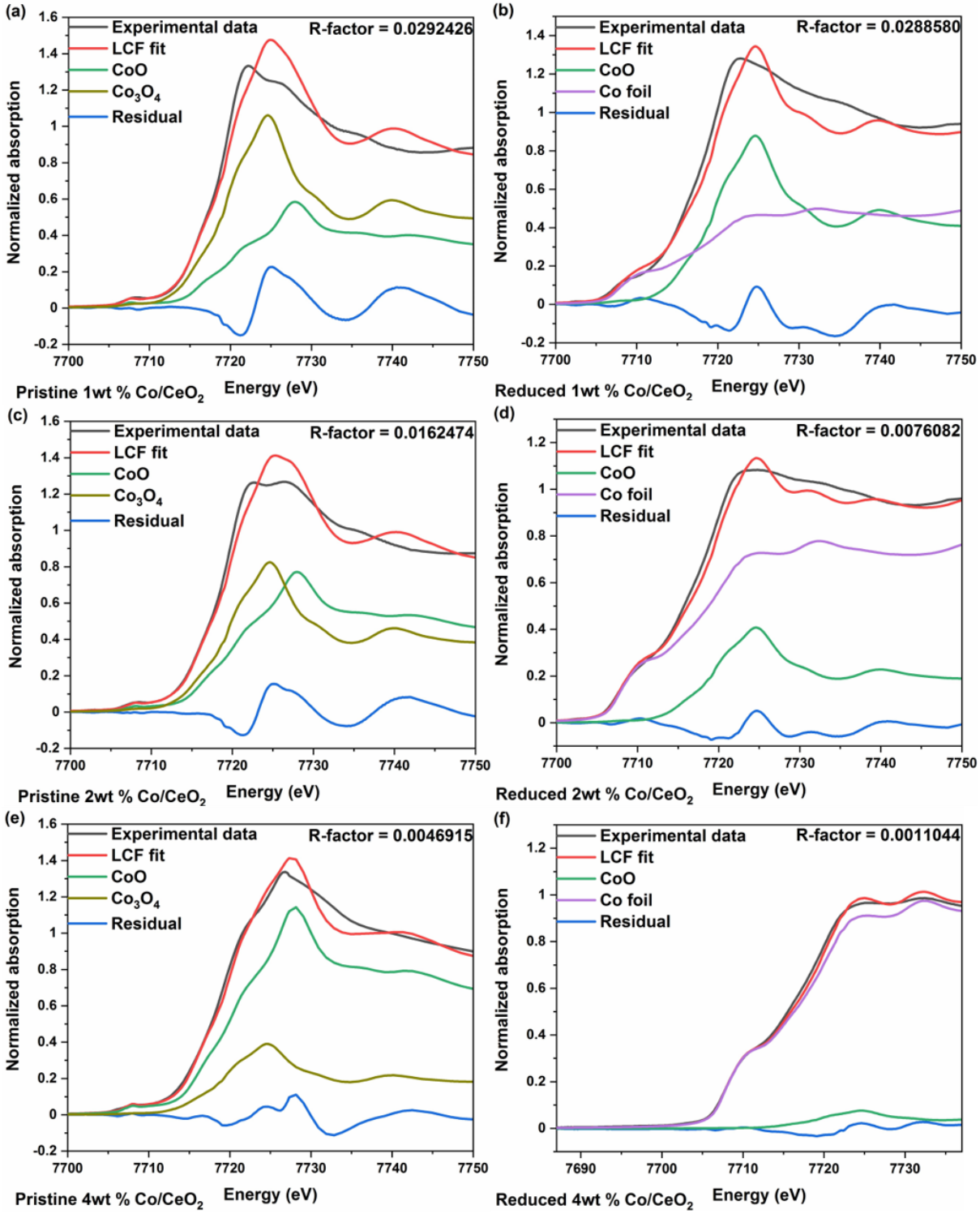

Figure S3.A. Linear combination fitting (LCF) on flattened μ(E) on Co *K* edge for 1wt% Co/CeO2 (a, b), 2wt% Co/CeO2 (c, d) and 4wt% Co/CeO2 (e, f) at pristine and reduced conditions.

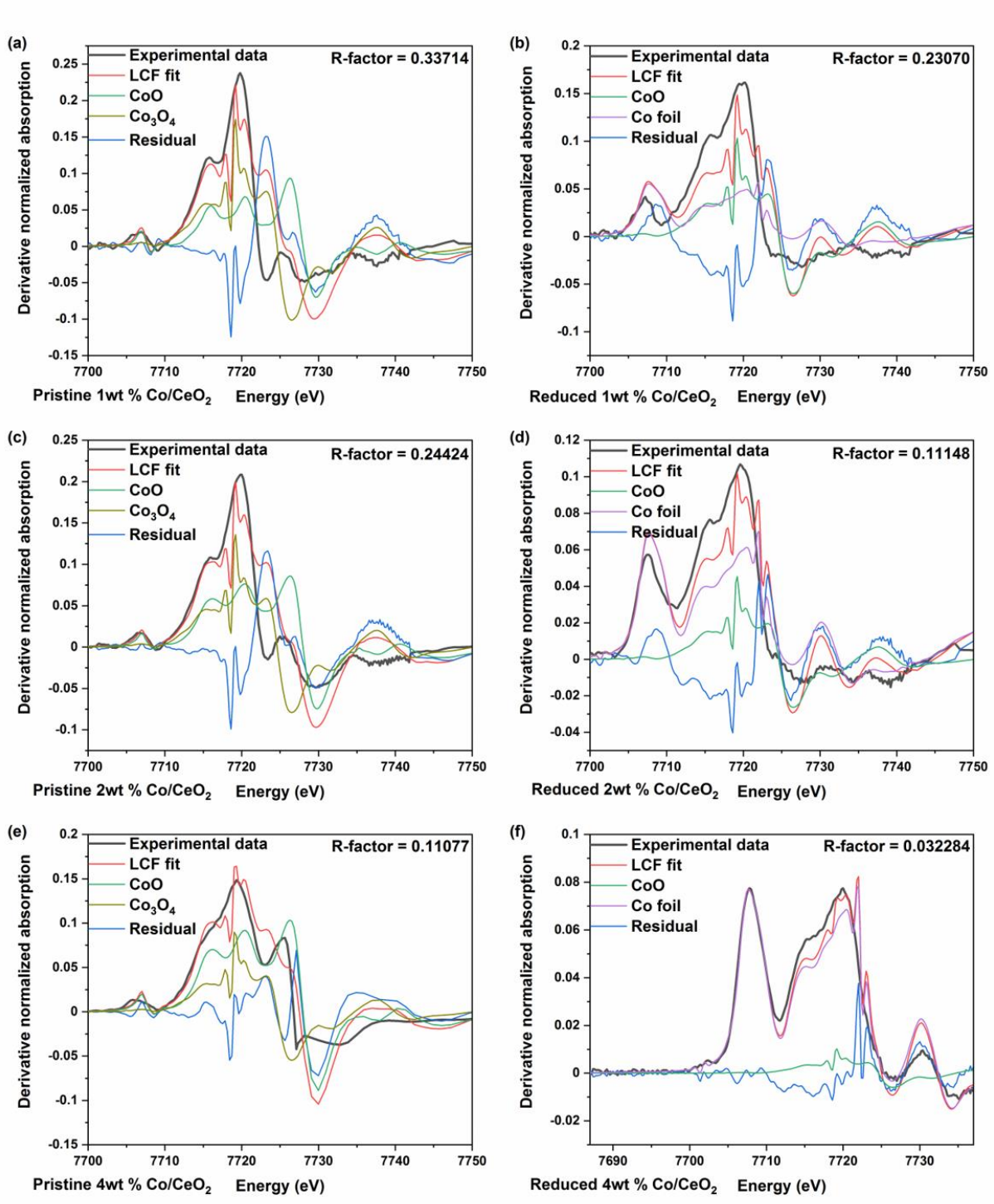

Figure S3.B. Linear combination fitting (LCF) on derivative flattened μ(E) on Co *K* edge for 1wt% Co/CeO_2 (a, b), 2wt% Co/CeO_2 (c, d) and 4wt% Co/CeO_2 (e, f) at pristine and reduced conditions.

Table S2.A. The composition of each phase determined by linear combination fitting (LCF) with flattened μ(E) and derivative flattened μ(E).

Spectra	Condition	Loading (wt%Co)	CoO (%)	Co_3O_4 (%)	Co foil (%)	R-factor
flattened μ(E)	Pristine	1	62	38	0	0.0292
Deriv. flattened μ(E)	Pristine	1	51	49	0	0.3371
flattened μ(E)	Reduced	1	51	0	49	0.0288
Deriv. flattened μ(E)	Reduced	1	30	0	70	0.2307
flattened μ(E)	Pristine	2	48	52	0	0.0162
Deriv. flattened μ(E)	Pristine	2	40	60	0	0.2442
flattened μ(E)	Reduced	2	24	0	76	0.0076
Deriv. flattened μ(E)	Reduced	2	13	0	87	0.1114
flattened μ(E)	Pristine	4	23	77	0	0.0046
Deriv. flattened μ(E)	Pristine	4	28	72	0	0.1107
flattened μ(E)	Reduced	4	4	0	96	0.0011
Deriv. flattened μ(E)	Reduced	4	3	0	97	0.0322

Table S2.B. The percentage difference of CoO phase between pristine and reduced conditions {(Pristine CoO - reduced CoO)/pristine CoO} determined by linear combination fitting (LCF) with flattened μ(E) and derivative flattened μ(E).

Sample	Change in CoO amount (%) in LCF of flattened μ(E)	Change in CoO amount (%) in LCF of deriv. flattened μ(E)
1wt% Co/CeO_2	18	41
2wt% Co/CeO_2	50	68
4wt% Co/CeO_2	83	89

EXAFS section

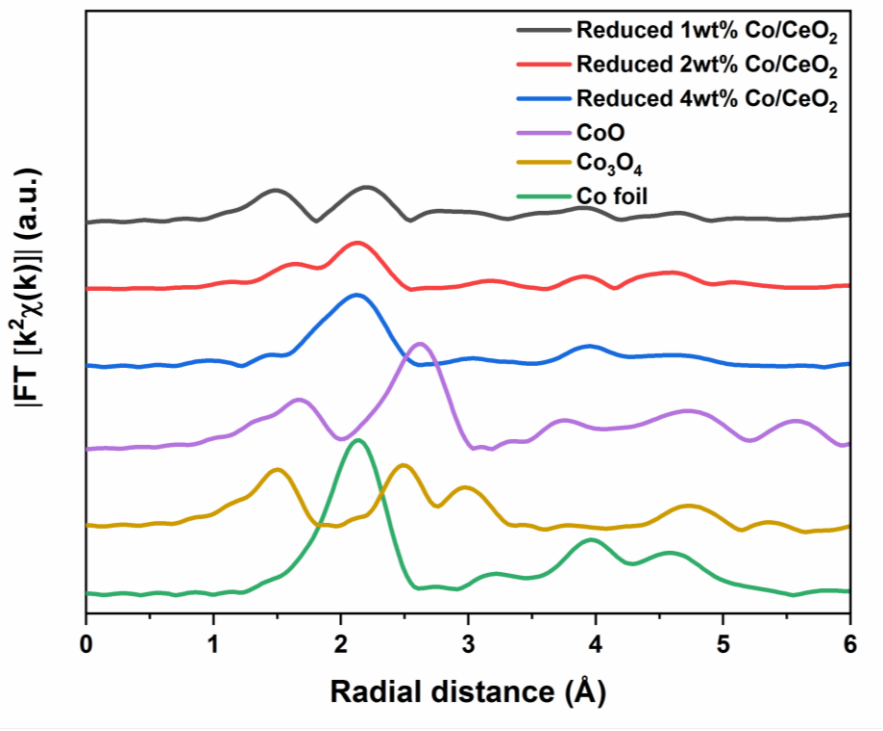

Figure S4.A. The magnitude of χ(R) in the Co *K* edge for reduced 1wt%, 2wt%, 4wt% Co/CeO_2, CoO, Co_3O_4 and Co foil.

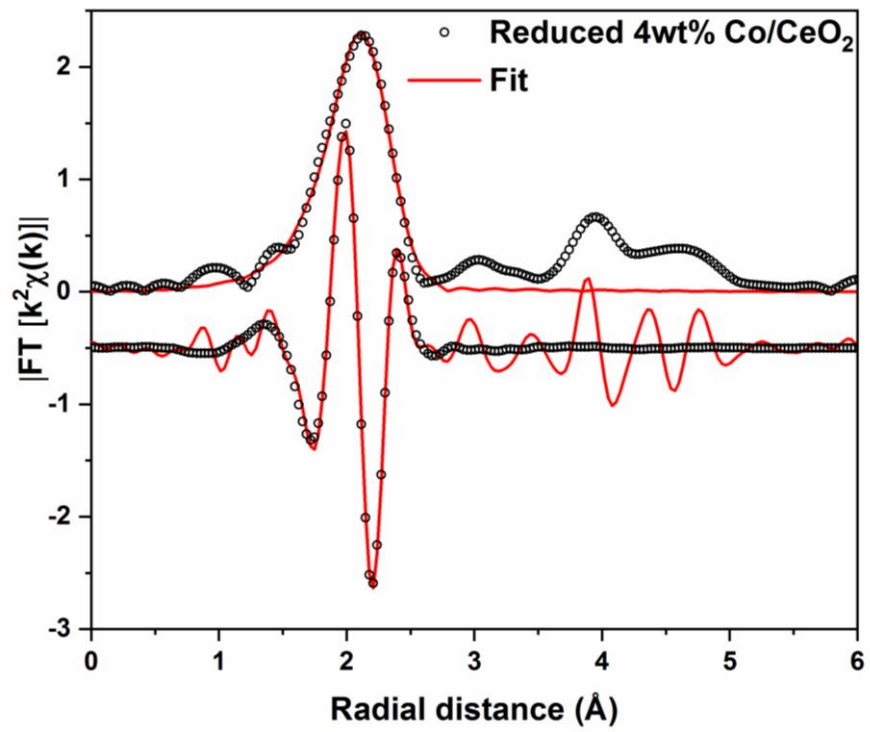

Figure S4.B. The fitting result in the Co-Co shell of χ(R) for reduced 4wt% Co/CeO_2

Table S3A The parameter values from the fitting result of χ(R) for reduce 4wt% Co/CeO_2

Sample	Shell	Bond length Å	Coordination Number	σ2 ($Å^2$)	E_0 shift (eV)	R-factor
Reduced 4wt%Co/CeO_2	Co-Co	2.49 ± 0.01	8.7 ± 0.7	0.010 ± 0.001	-1.3	0.008

Table S3B. The relationship between the first shell coordination number and the particle size using the half sphere particle model for a metal with a fcc structure[1].

First shell Coordination Number	**Size (nm)**
6.32	1.3
7.39	1.8
8.41	2.2
9.05	2.7
9.27	2.9
9.6	3.3

The analysis on the Co-O bond length using EXAFS data

A typical form of the EXAFS function is given by[2, 3]:

$$\chi(\mathrm{k}) = \sum_{R} N_R S_0^2 \frac{|f(k)|}{kR^2} e^{\frac{-2R}{\lambda(k)}} e^{-2\sigma^2 k^2} \sin(2kR + 2\delta_C + \Phi)$$

In the function: R is interatomic distances, N_R is the coordination number, σ^2 is mean-square relative displacement $f(k) = |f(k)|e^{i\Phi(k)}$ is the backscattering amplitude. δ_C and Φ are phase shifts for the absorber and backscatterer. λ(k) is the energy dependent XAFS mean free path. S_0^2 is a many-body amplitude reduction factor.

As for the system in this study, the χ(k) contribution from the Co-O first shell can be isolated by Fourier filtering which has been demonstrated in literature[4, 5]. The $k^3\chi(k)$ is used to make first shell easier to separate from the second shell in the χ(R), as shown in **Figure S4C**, the R space region of 1.3 ~ 1.8 Å for 1wt% and 2wt% Co/CeO_2 and 1.3 ~ 2.0 Å for CoO reverse in Fourier transform. And the phase part corresponding to ($2kR_{Co\text{-}O} + \delta_c(k) + \Phi(k)$) were obtained in the Athena and plotted as a function of q(Å^{-1}) in **Figure S4C(b),** the q maximum (12 Å^{-1}) is smaller than the one used in the forward Fourier transform to avoid Fourier filtering errors[5]. It has been shown in literature that the phase shifts ($2\delta_C + \Phi$) in EXAFS are essentially independent of chemical environment for photoelectron energies > 100 eV ≈ 5.1 Å^{-1}. And the interatomic distances can be determined typically to accuracies of 0.02 A[6]. Therefore, the $R_{Co\text{-}O}$ of CoO was used as a reference to cancel out the phase shifts from the samples.

And the $\Delta R_{Co\text{-}O}$ of samples can be calculated by: $\Delta R_{Co-O} = \frac{\mathrm{Pha}[k^3\chi(\mathrm{q})]_{sample} - \mathrm{Pha}[k^3\chi(\mathrm{q})]_{CoO}}{2q}$ as shown in Figure S4C(c). The same process was used to evaluate the $\Delta R_{Co\text{-}O}$ of $Co(OH)_2$ from its standard spectra obtained from Farrel Lytle Database. Our data analysis on standard $Co(OH)_2$ spectra demonstrates the bond length can be determined by the method to 0.02 Å accuracy. According to our calculation using Feff[2, 7, 8] on standard CoO and $Co(OH)_2$ structure, the Co-O bond length results are: $R_{Co\text{-}O}$ (CoO) = 2.14 Å, $R_{Co\text{-}O}$ ($Co(OH)_2$) = 2.10 Å.

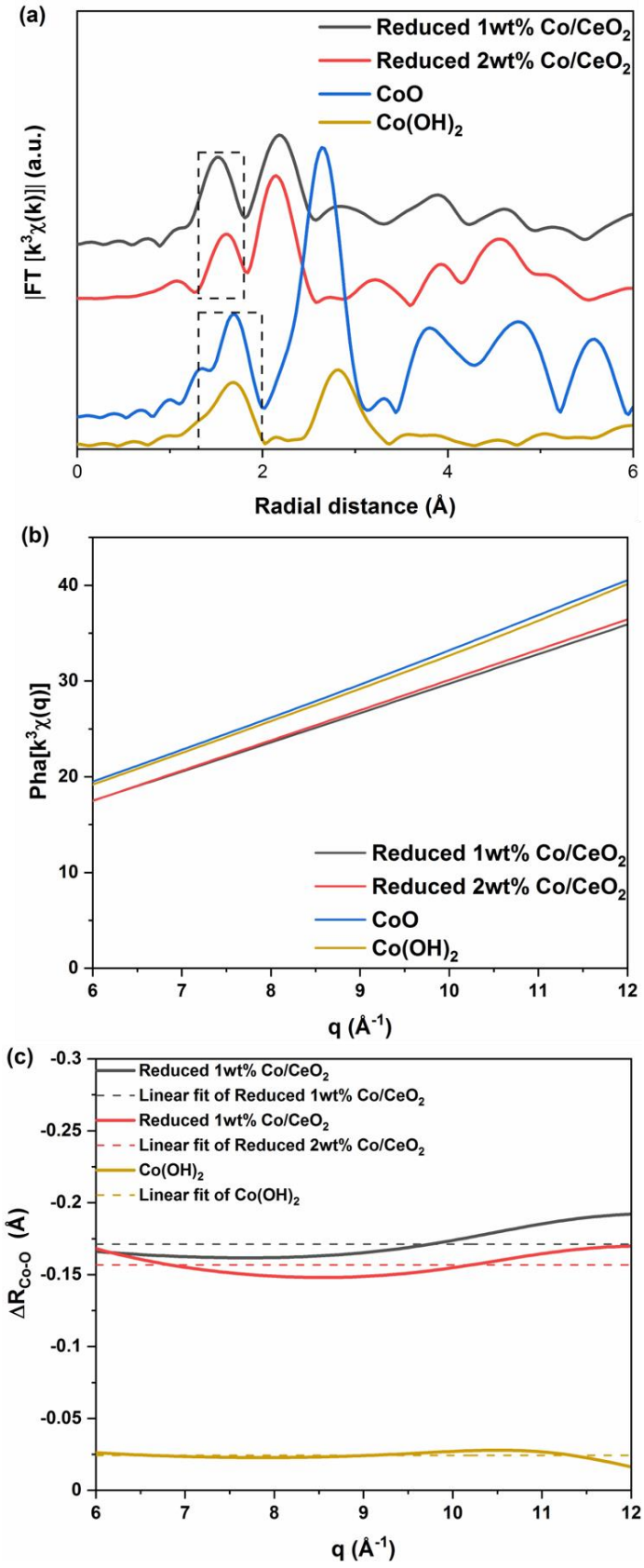

Figure S4C. The Fourier transfer results of $k^3\chi(k)$ (a) the phase part Pha[$k^3\chi(q)$] from Fourier filtering (b) the $\Delta R_{Co\text{-}O}$ analyzed from the phase part of Fourier filtering using $R_{Co\text{-}O}$ (CoO) as reference $\Delta R_{Co\text{-}O}$ ($R_{Co\text{-}O}$ (sample) - $R_{Co\text{-}O}$ (CoO)) (c) for 1wt%Co/CeO_2, reduced 2wt%Co/CeO_2 and $Co(OH)_2$

Table S3C. The linear fitting results using a line with 0 slope on ΔR_{Co-O} (R_{Co-O} (sample) - R_{Co-O} (CoO)), the XAS spectra of standard $Co(OH)_2$ is from Farrel Lytle Database

Sample	ΔR_{Co-O} from fitting	R_{Co-O} (with R_{Co-O} (CoO) = 2.14 Å)	Residual sum of squares
1wt%Co/CeO_2	-0.17	1.97	0.0128
2wt%Co/CeO_2	-0.16	1.98	0.0063
$Co(OH)_2$	-0.02	2.12	0.0006

In situ DRIFTS for flow system

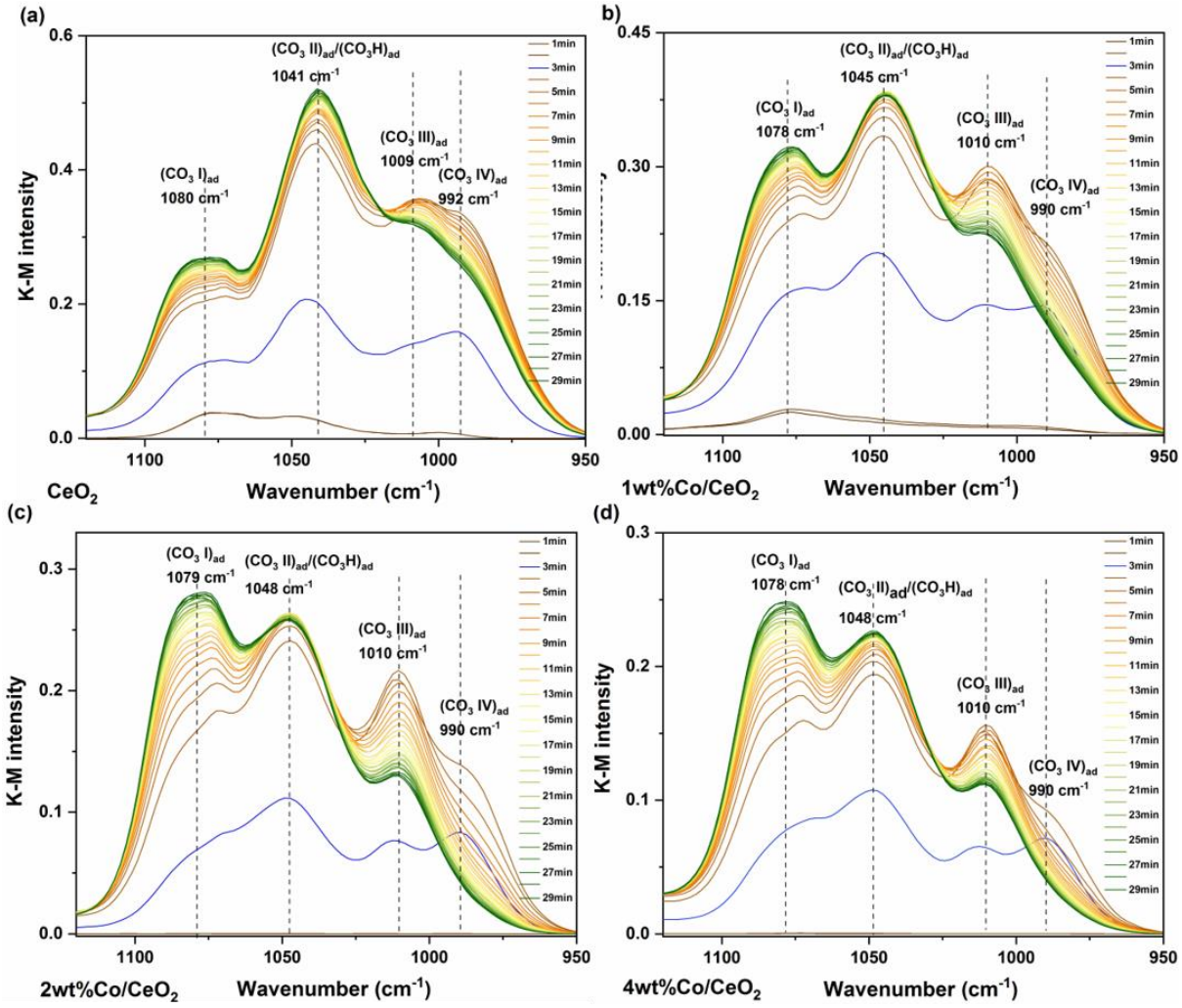

Figure S5. The evolution of signal in the region of carbonate and hydrogen carbonate ν(CO) bands collected during *in situ* DRIFTS **flow** experiments for (**a**) CeO_2, (**b**) 1wt%Co/CeO_2, (**c**) 2wt%Co/CeO_2 and (**d**) 4wt%Co/CeO_2.

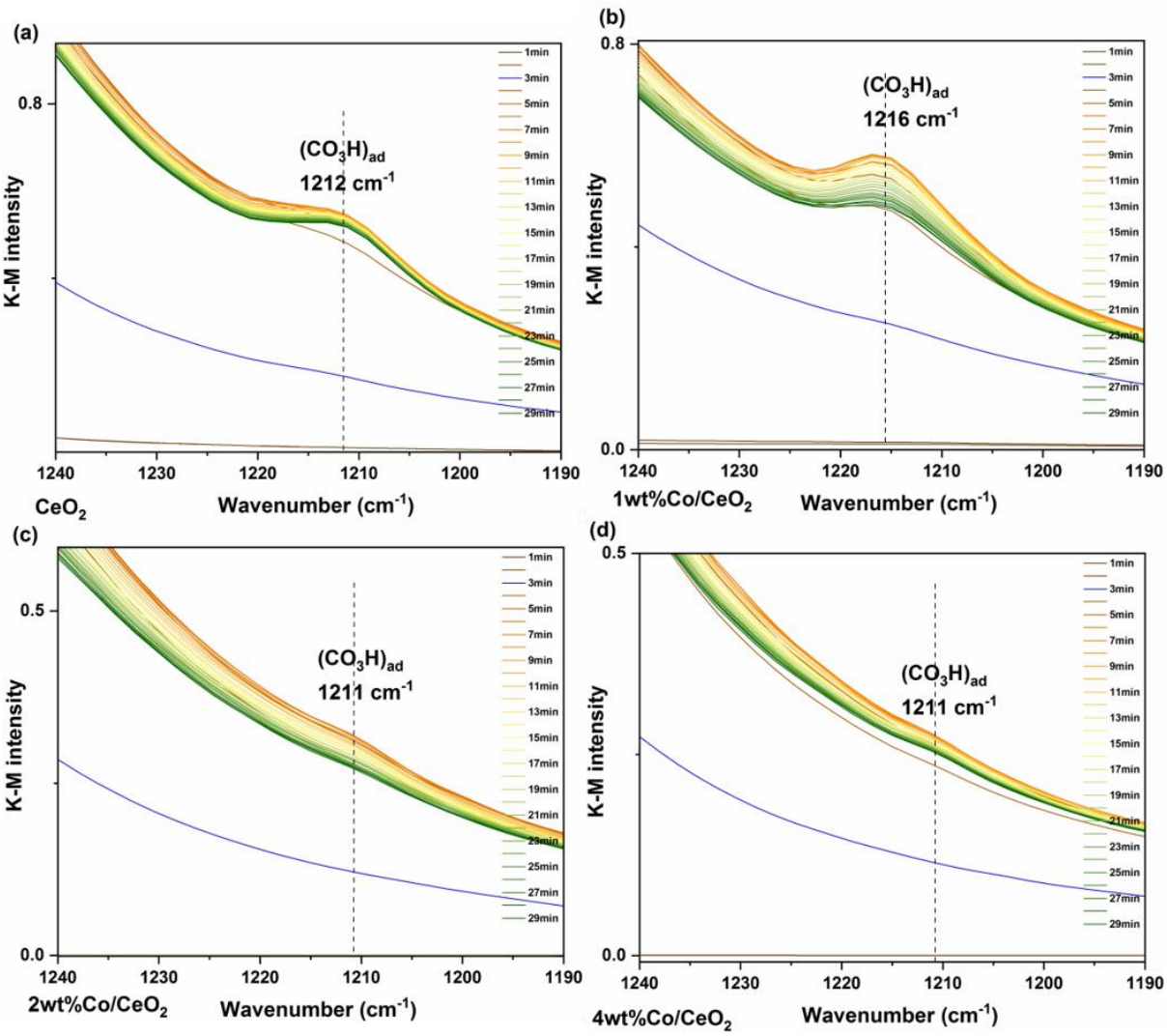

Figure S6. The evolution of signals in the region of hydrogen carbonate δ(COH) collected during *in situ* DRIFTS **flow** experiments for (**a**) plain CeO_2, (**b**) 1wt%Co/CeO_2, (**c**) 2wt%Co/CeO_2 and (**d**) 4wt%Co/CeO_2.

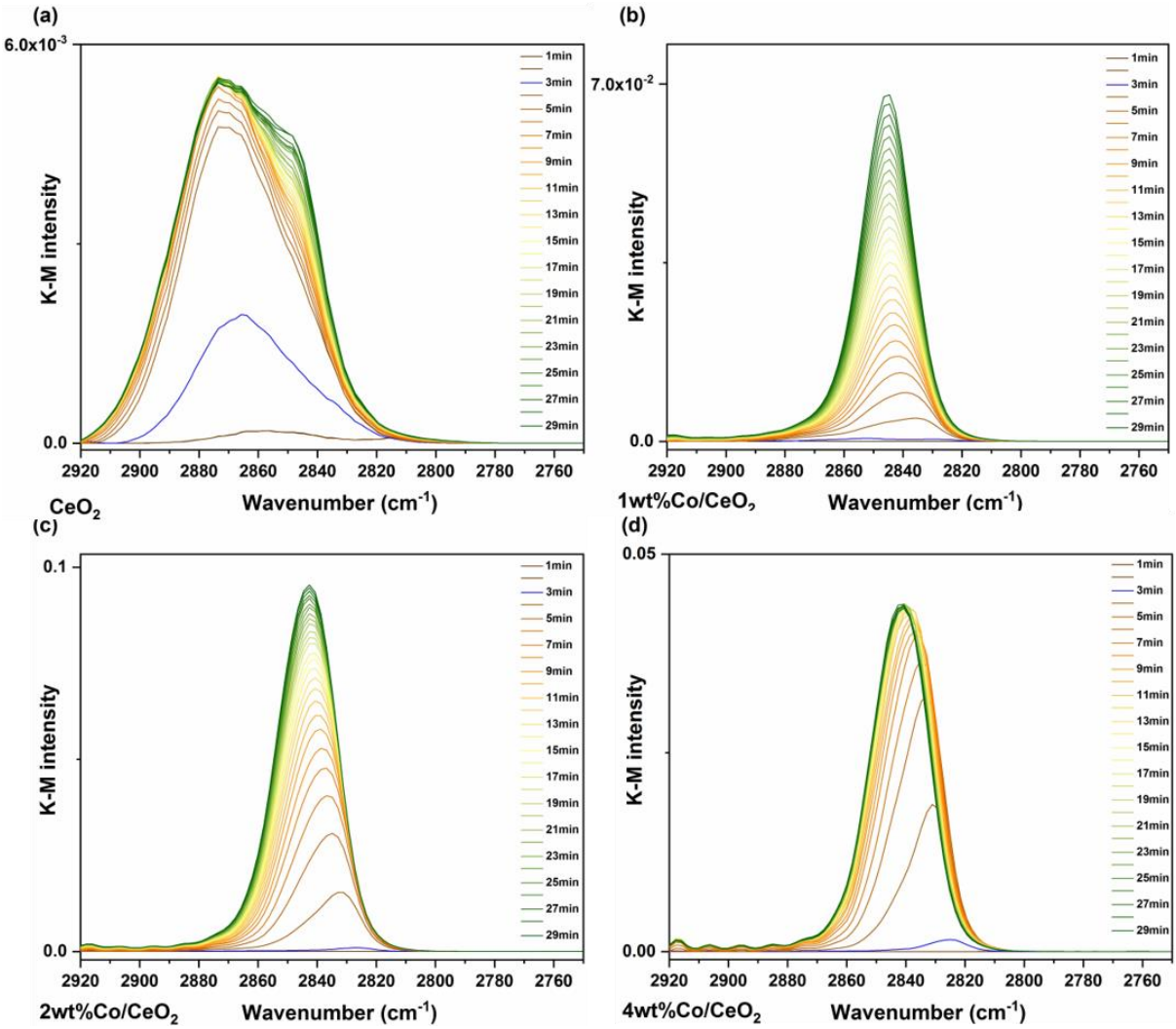

Figure S7. *In situ* DRIFTS data collected in **flow** experiments for (**a**) plain CeO_2, (**b**) 1wt%Co/CeO_2, (**c**) 2wt%Co/CeO_2 and (**d**) 4wt%Co/CeO_2 in the region of 2750-2920 cm^{-1}.

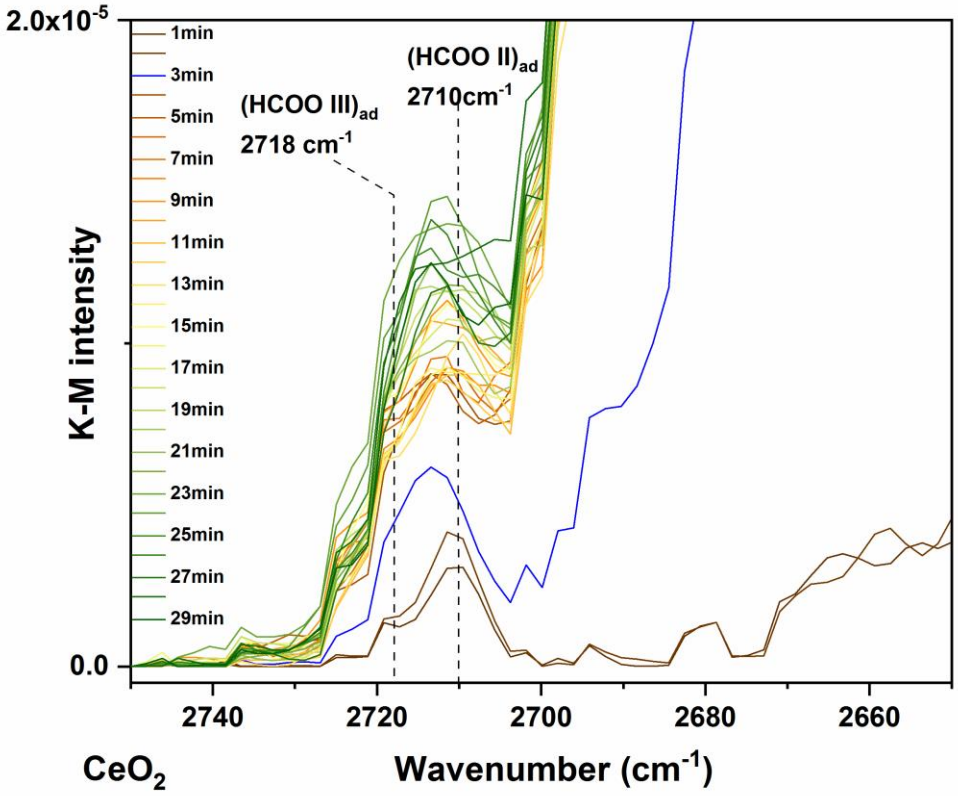

Figure S8. *In situ* DRIFTS data collected in flow experiments for CeO_2 at the 2650-2750 cm^{-1} region.

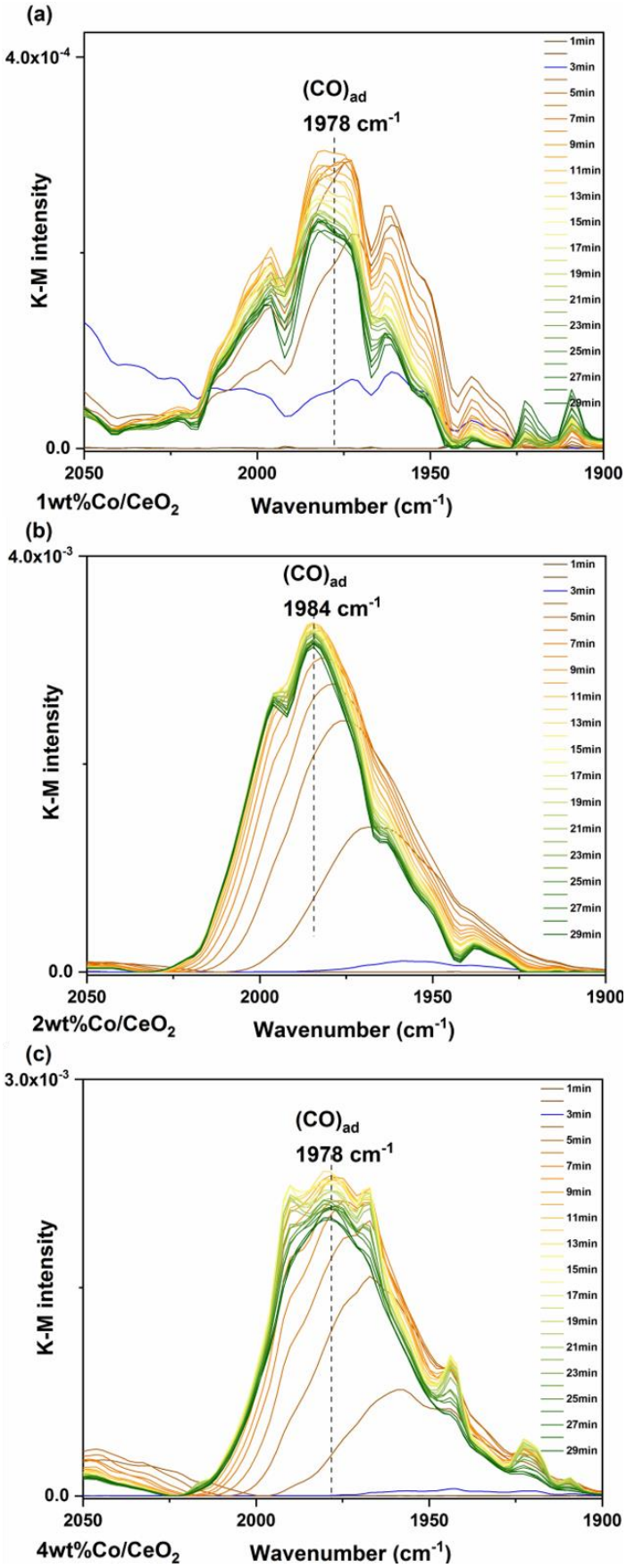

Figure S9. The evolution of signals in the region of the CO ν(CO) band collected during *in situ* DRIFTS **flow** experiments for (**a**) 1wt%Co/CeO_2, (**b**) 2wt%Co/CeO_2 and (**c**) 4wt%Co/CeO_2.

In situ DRIDTS for closed system

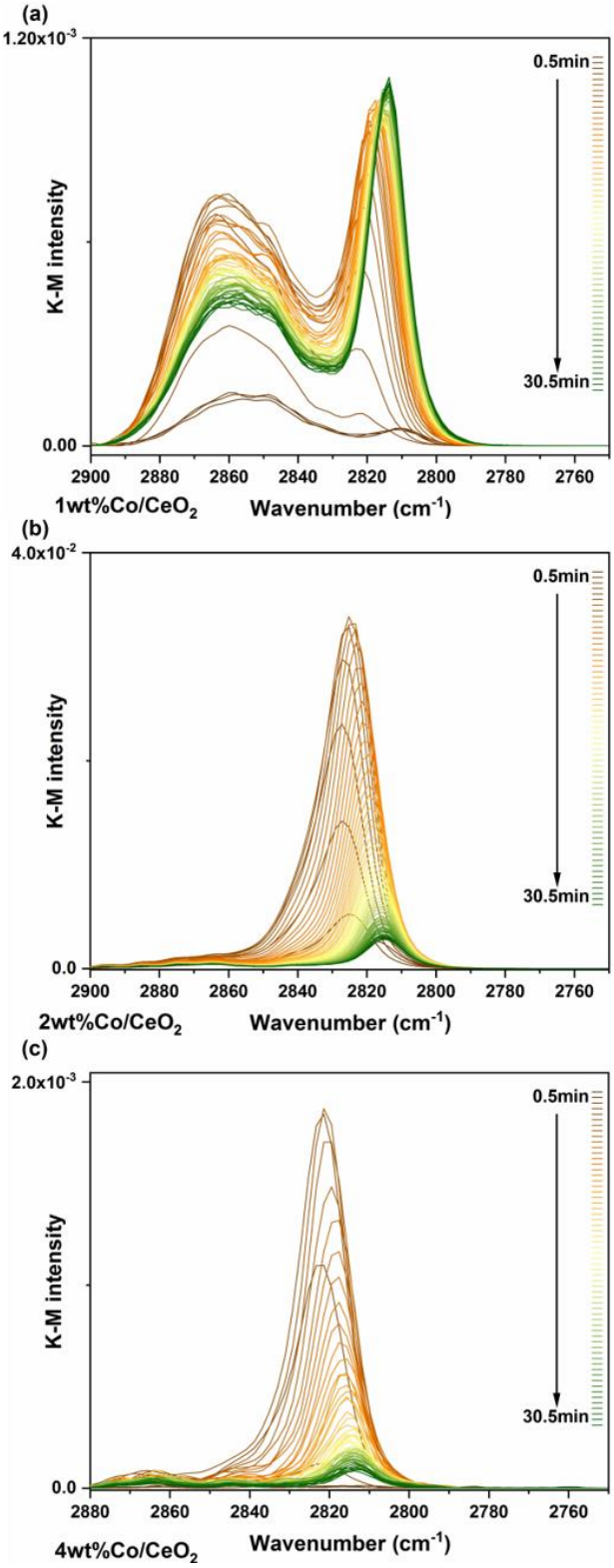

Figure S10. The evolution of signal in the region of 2750-2880 cm^{-1} collected during *in situ* DRIFTS **closed-system** experiments for (**a**) 1wt%Co/CeO_2, (**b**) 2wt%Co/CeO_2 and (**c**) 4wt%Co/CeO_2.

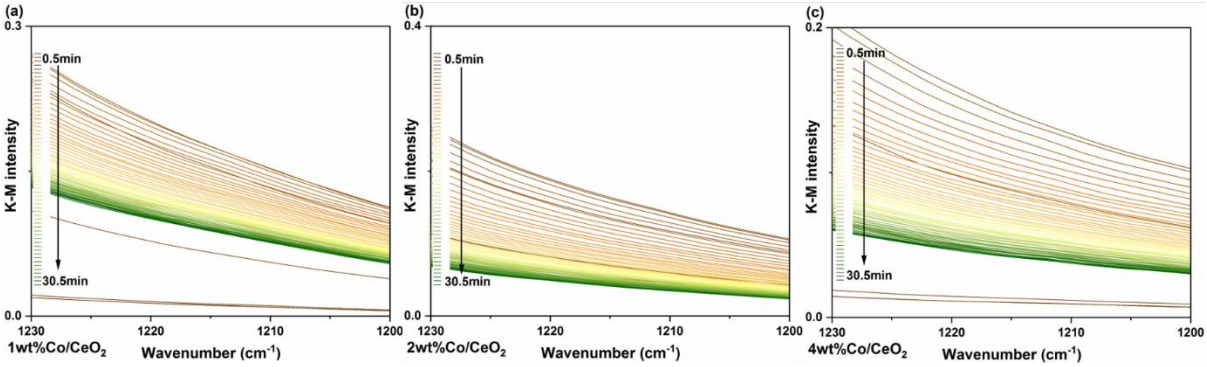

Figure S11. The evolution of signal in the region of the hydrogen carbonate δ(COH) band collected during *in situ* DRIFTS closed-system experiments for (**a**) 1wt%Co/CeO_2, (**b**) 2wt%Co/CeO_2 and (**c**) 4wt%Co/CeO_2 catalysts.

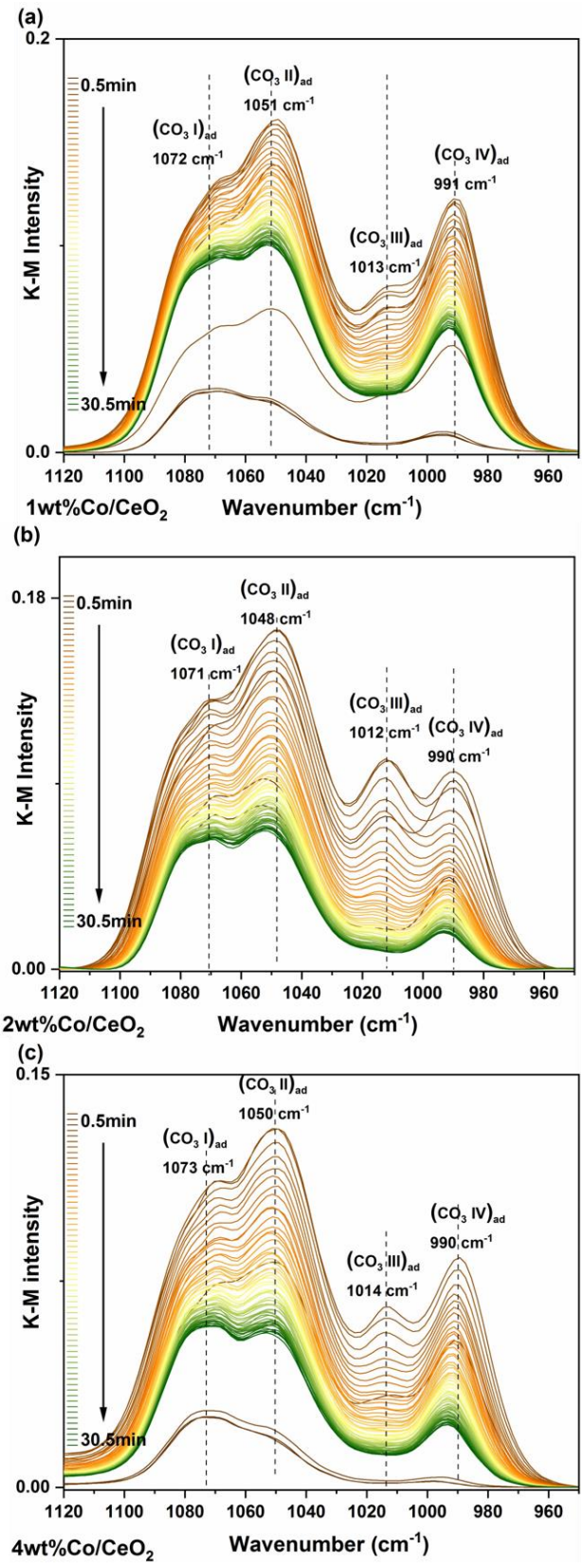

Figure S12. The evolution of carbonate and hydrogen carbonate ν(CO) bands collected during *in situ* DRIFTS in **closed-system** experiments. (**a**) 1wt%Co/CeO_2, (**b**) 2wt%Co/CeO_2, (**c**) 4wt%Co/CeO_2

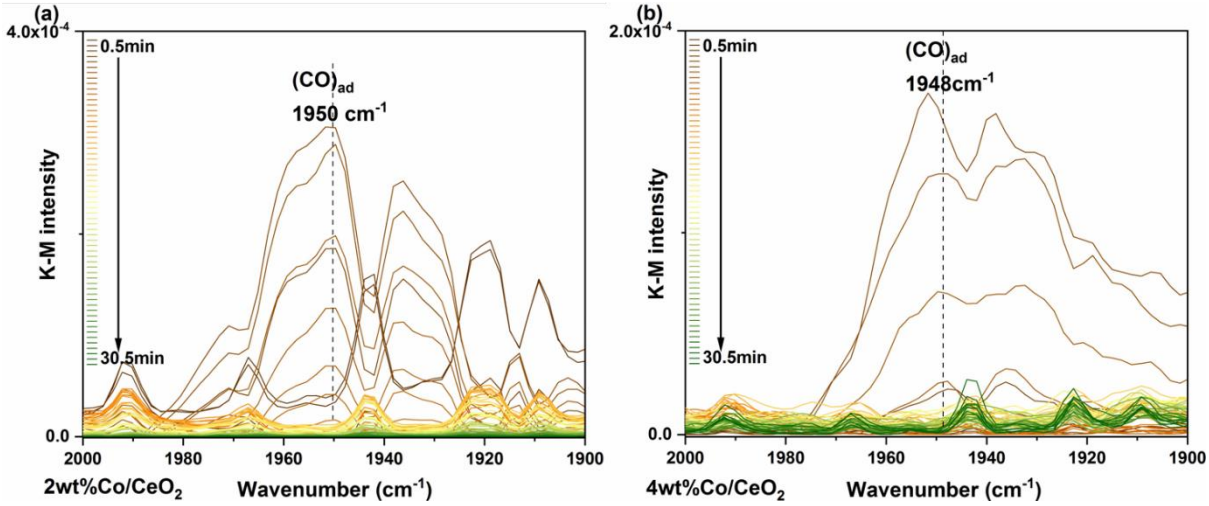

Figure S13. The evolution of signal in the region of 1900-2000 cm^{-1} (adsorbed CO ν(CO) band) collected during *in situ* DRIFTS **closed-system** experiments. (a) 1wt%Co/CeO_2, (b) 2wt%Co/CeO_2

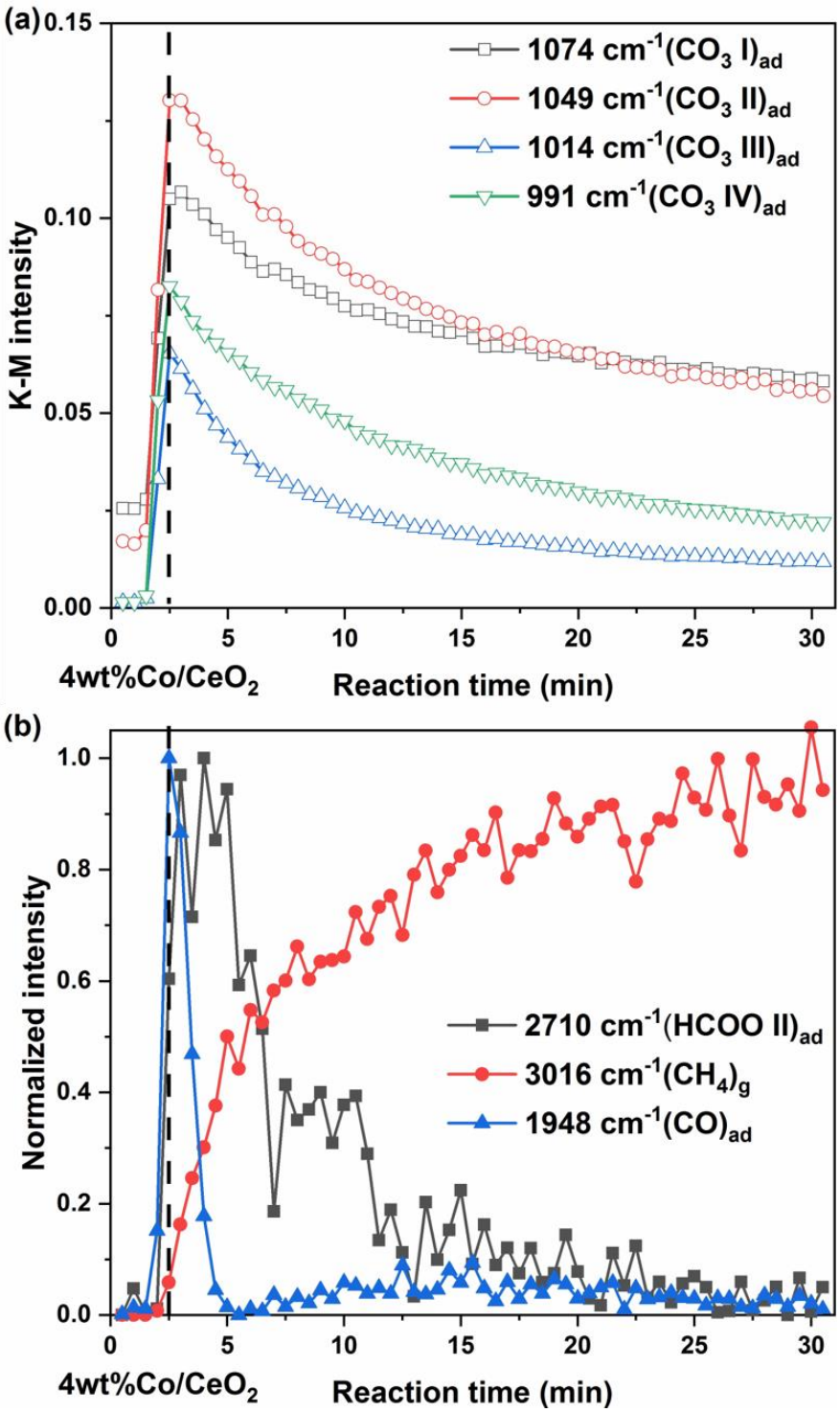

Figure S14, Evolution of (**a**) carbonate species (**b**) formate, adsorbed CO and CH_4 gas phase for 4wt%Co/CeO_2 catalyst, with corresponding normalized peak intensity, derived from *in situ* DRIFTS experiments on **closed-system** at 250 ºC, 1atm pressure. Approximate 1v%CO_2 in H_2 was introduced into the cell before valves were switched off. The highest CO_2 concentration was observed at 2.5 min (marked with dash).

Summary of relevant peak assignments in the literature

Table S4 Summary of peak assignments (in wavenumber cm^{-1}) for adsorbed carbonate and formate according to the literature.

Carbonate			ν (CO)	ν (CO)	ν (CO)	ν (CH)	δ(OCH)	δ(COH)	Conbination band	Ref.
Bidentate carbonate			1567	1289	1014					9
			1566	1300	1019					10
			1563	1296	1015					11
	Tridentate carbonate		1568-1596	1286-1303	990-1018				~2850	12
Polydentate /or monodentate carbonate			1465	1359	1080					10
			1456	1348	1040					11
			1462	1353	1066					13
	Tridentate carbonate	Ce^{3+}	1490	1380	1085					12
		Ce^{4+}	1451-1500	1342-1380	1038-1065				~2876	
Hydrogen carbonate		I	1599	1413	1025			1218		13
		II	1613	1391	1045			1218		
			1609	1395	1044			1217		10
formate			1558	1329		2852	1369			9
			1584	1330		2838	1375			10
			1547-1561	1360-1358		2845-2850	1372-1373		2935, 2725	12
	I (on Ce^{3+})		1580	1335			~1370			14
	II (on Ce^{3+})		1561	1356			~1370			
	III (on Ce^{4+})		1550	1371			~1370			

References

1. A. M. Beale and B. M. Weckhuysen, *Physical Chemistry Chemical Physics*, 2010, **12**, 5562-5574.
2. J. J. Rehr and R. C. Albers, *Reviews of Modern Physics*, 2000, **72**, 621-654.
3. P. A. O'Day, J. J. Rehr, S. I. Zabinsky and G. E. Brown, Jr., *Journal of the American Chemical Society*, 1994, **116**, 2938-2949.
4. E. A. Stern, B. A. Bunker and S. M. Heald, *Physical Review B*, 1980, **21**, 5521-5539.
5. D. C. Koningsberger, B. L. Mojet, G. E. van Dorssen and D. E. Ramaker, *Topics in Catalysis*, 2000, **10**, 143-155.
6. P. H. Citrin, P. Eisenberger and B. M. Kincaid, *Physical Review Letters*, 1976, **36**, 1346-1349.
7. J. J. Rehr, J. J. Kas, M. P. Prange, A. P. Sorini, Y. Takimoto and F. Vila, *Comptes Rendus Physique*, 2009, **10**, 548-559.
8. J. J. Rehr, J. J. Kas, F. D. Vila, M. P. Prange and K. Jorissen, *Physical Chemistry Chemical Physics*, 2010, **12**, 5503-5513.
9. C. Li, Y. Sakata, T. Arai, K. Domen, K.-i. Maruya and T. Onishi, *Journal of the Chemical Society, Faraday Transactions 1: Physical Chemistry in Condensed Phases*, 1989, **85**, 1451-1461.
10. O. Pozdnyakova, D. Teschner, A. Wootsch, J. Kröhnert, B. Steinhauer, H. Sauer, L. Toth, F. C. Jentoft, A. Knop-Gericke, Z. Paál and R. Schlögl, *Journal of Catalysis*, 2006, **237**, 17-28.
11. C. Binet, A. Badri, M. Boutonnet-Kizling and J.-C. Lavalley, *Journal of the Chemical Society, Faraday Transactions*, 1994, **90**, 1023-1028.
12. G. N. Vayssilov, M. Mihaylov, P. S. Petkov, K. I. Hadjiivanov and K. M. Neyman, *The Journal of Physical Chemistry C*, 2011, **115**, 23435-23454.
13. C. Binet, M. Daturi and J.-C. Lavalley, *Catalysis Today*, 1999, **50**, 207-225.
14. P. G. Lustemberg, M. V. Bosco, A. Bonivardi, H. F. Busnengo and M. V. Ganduglia-Pirovano, *The Journal of Physical Chemistry C*, 2015, **119**, 21452-21464.